Electronic Supplementary Information

Ultrasmall Mo_2C nanocrystals embedded in N-doped porous carbons as surface-dominated capacitive anode for lithium-ion capacitors

Xufei Liu,[a] Xiaofang Zhang,[b] Yu Dou,[a] Peng Mei,[b] Xiaolan Ma[a] and Yingkui Yang*[ab]

[a] *Key Laboratory of Catalysis and Energy Materials Chemistry of Ministry of Education & Hubei Key Laboratory of Catalysis and Materials Science, South-Central University for Nationalities, Wuhan 430074, China*
E-mail: ykyang@mail.scuec.edu.cn

[b] *Hubei Engineering Technology Research Centre of Energy Polymer Materials, School of Chemistry and Materials Science, South-Central University for Nationalities, Wuhan 430074, China*

Experimental section

Materials

Pyromellitic dianhydride (PMDA) and 4, 4'-methylenedianiline (MDA) were obtained from Aladdin Industrial Corporation (Shanghai, China). Anhydrous ethylene diamine (EDA) and phosphomolybdic acid (PMo_{12}) were supplied by Sinopharm Chemical Reagent Limited Corporation. All chemicals were used without further purification.

Synthesis of Mo_2C@NCB, Mo_2C@NCS, NCB, and NCS

Typically, PMDA (2 mmol, 436.2 mg) was dissolved in 50 mL deionized water, and an equimolar diamine (MDA or EDA) was then added to obtain a comonomer salt by stirring overnight at room temperature. To the comonomer salt (solid: 750 mg) solution was added PMo_{12} (250 mg), and the resultant mixture was transferred into a 100 mL Teflon-inner autoclave and heated at 200°C for 12 h. After cooling down naturally, the products were collected by filtrating, washing with deionized water and ethanol, and drying overnight, yielding Mo-containing polyimide precursors. Mo_2C@NCB and Mo_2C@NCS were finally obtained by calcination of the Mo-containing polyimides derived from PMDA-MDA and PMDA-EDA at 350°C for 2h and then 800°C for 2 h under Ar flowing, respectively. In particular, the loading amount of Mo_2C in Mo_2C@NCB was adjusted by changing the mass feed ratio of PMo_{12} to PMDA-MDA comonomer salts into 1:1.5, 1:3, and 1:6. Similarly, NCB and NCS were also produced by identical experiments in the absence of PMo_{12} using pure polyimides derived from PMDA-MDA and PMDA-EDA, respectively.

General characterization

The morphologies were acquired from analyzed by transmission electron microscope (TEM, Tecnai G2 20 S-TWIN), and scanning electron microscopy (SEM, SU8010). Energy dispersed X-ray spectroscopy (EDS) was performed on scanning transmission electron microscopy (STEM, Talos F200X). The Nitrogen adsorption/desorption isotherms were measured by ASAP 2020 Plus, specific

surface area (SSA) and pore volumes were calculated based on the Brunauer-Emmett-Teller (BET) model and nonlocal density functional theory (DFT), respectively. Before adsorption measurements, all the samples were degassed at 350°C for 24 h under vacuum. X-ray photoelectron spectra (XPS) were determined by an X-ray photoelectron spectrometer with an excitation source of Mg Kα on ESCALAB Xi^+. Crystalline structures were recorded on a D8 Advance X-ray diffraction (XRD) with a scan rate of 10° min^{-1}. Raman spectra were collected on a Renishaw spectrometer with an excitation laser of λ = 532 nm. Thermo gravimetric analysis (TGA) was tested via Netzsch TG 209 F3 Tarsus, with a heating rate of 10 ˚C min^{-1} under an air atmosphere. In particular, the loading level of Mo_2C in Mo_2C@NCB and Mo_2C@NCS was calculated according to the method reported previously.[1]

Electrochemical measurements

The working electrodes were fabricated by mixing active materials (80%), super P (10%), and polyvinylidene fluoride (10%) in NMP, obtaining the slurry followed by blade-coating onto the corresponding current collector (using Al foil for the cathode and Cu foil for the anode, respectively). After drying at 80°C for 12 h, the electrodes were punched into 10 mm disks in diameter, and the loading mass of active materials was around 4–6 mg cm^{-2} on each electrode. Coin-type cells for LIBs were assembled in the Ar-filled glove box, and lithium foil, Celgard-2400, and 1 M $LiPF_6$ in EC/DEC/DMC (1:1:1 in volume) were employed as the counter electrode, separator, and electrolyte, respectively. As for LICs, NCB was selected as the cathode material. Of note, the Mo_2C@NCB and Mo_2C@NCS based anodes were pre-lithiated by charging/discharging for 10 cycles at 0.1 A g^{-1} and discharged to 0.01 V. The mass ratio of cathode/anode in LICs was adjusted in the range of 1:1 to 4:1. The electrochemical performance was tested on a Land CT 2001A automatic battery tester (Wuhan, China) in the voltage range of 0.01–3 V. The cyclic voltammetry (CV) plot and electrochemical impendence spectroscopy (EIS) tests were investigated on a CHI660E (Chenhua, China) electrochemical work station at room temperature.

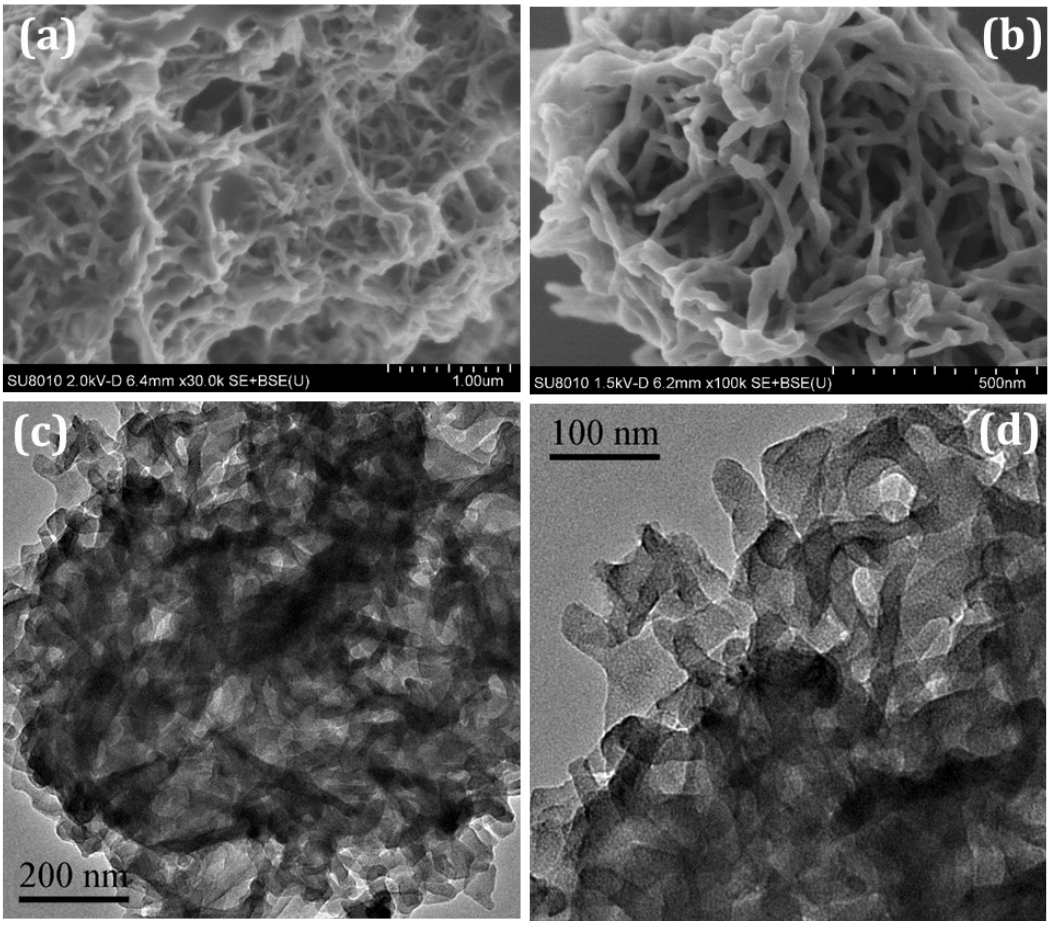

Fig. S1 SEM (a, b) and TEM (c, d) images of nitrogen-doped carbon nanobelts (NCB).

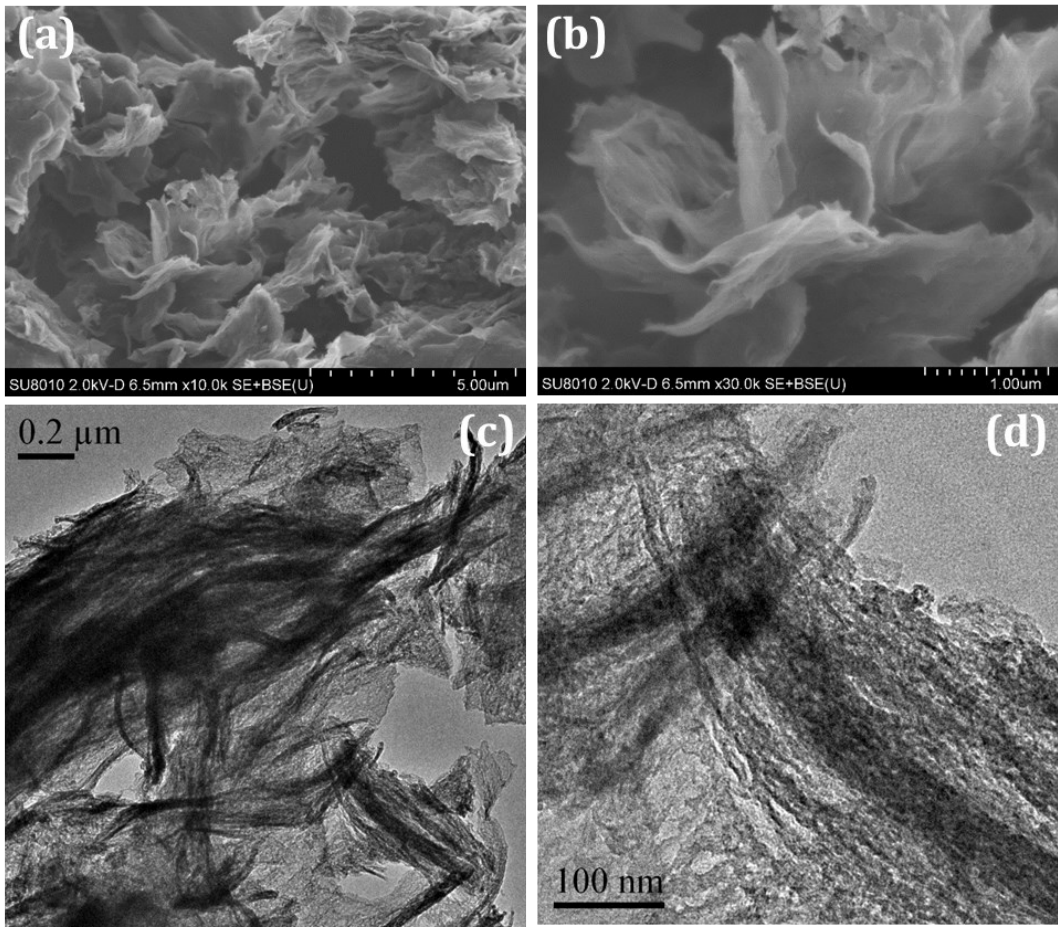

Fig. S2 SEM (a, b) and TEM (c, d) images of nitrogen-doped carbon nanosheets (NCS).

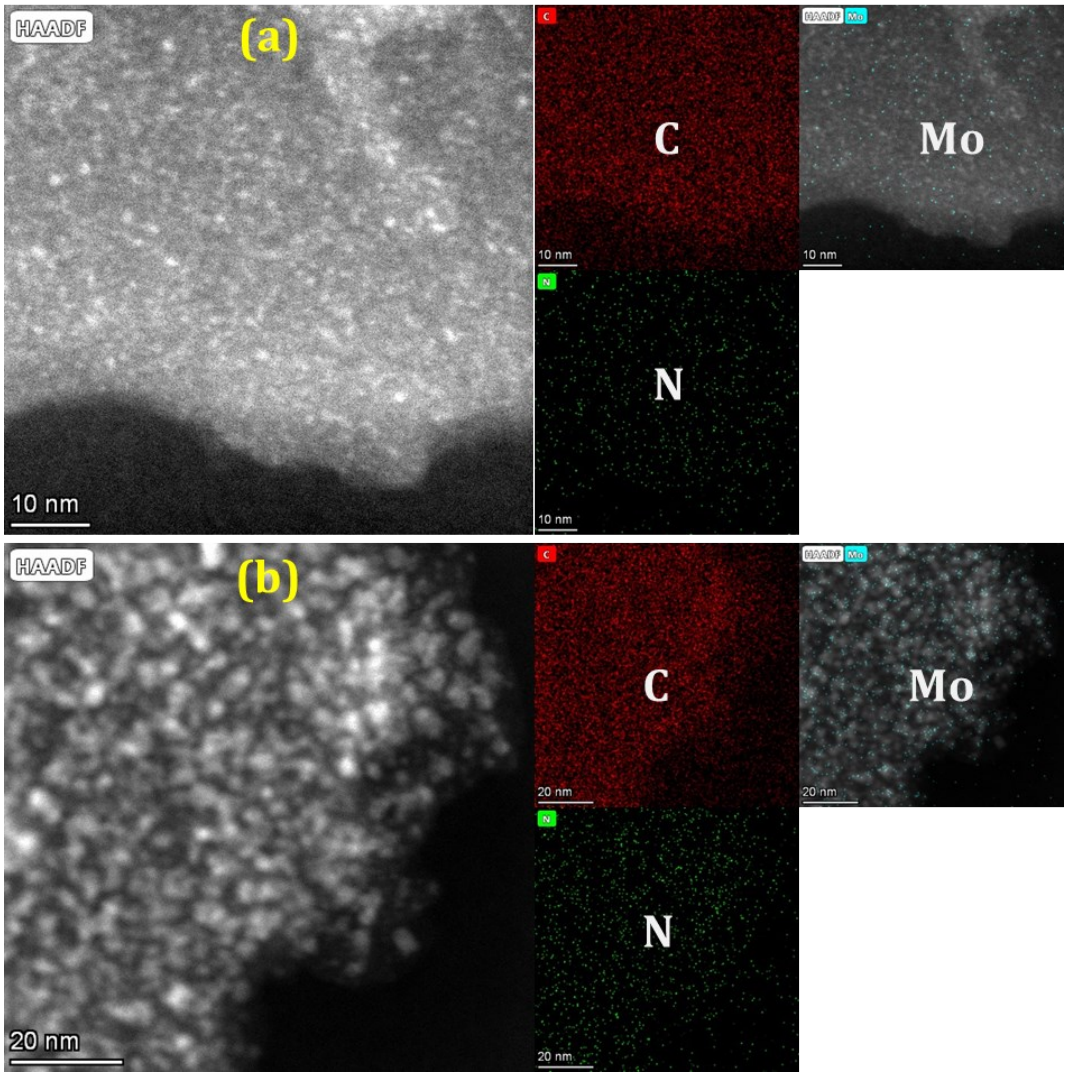

Fig. S3 STEM images and the corresponding elemental mappings of C, Mo, N, of (a) Mo_2C@NCB and (b) Mo_2C@NCS derived from the feed ratio of 1:3 for PMo_{12} to PMDA-MDA comonomer salts.

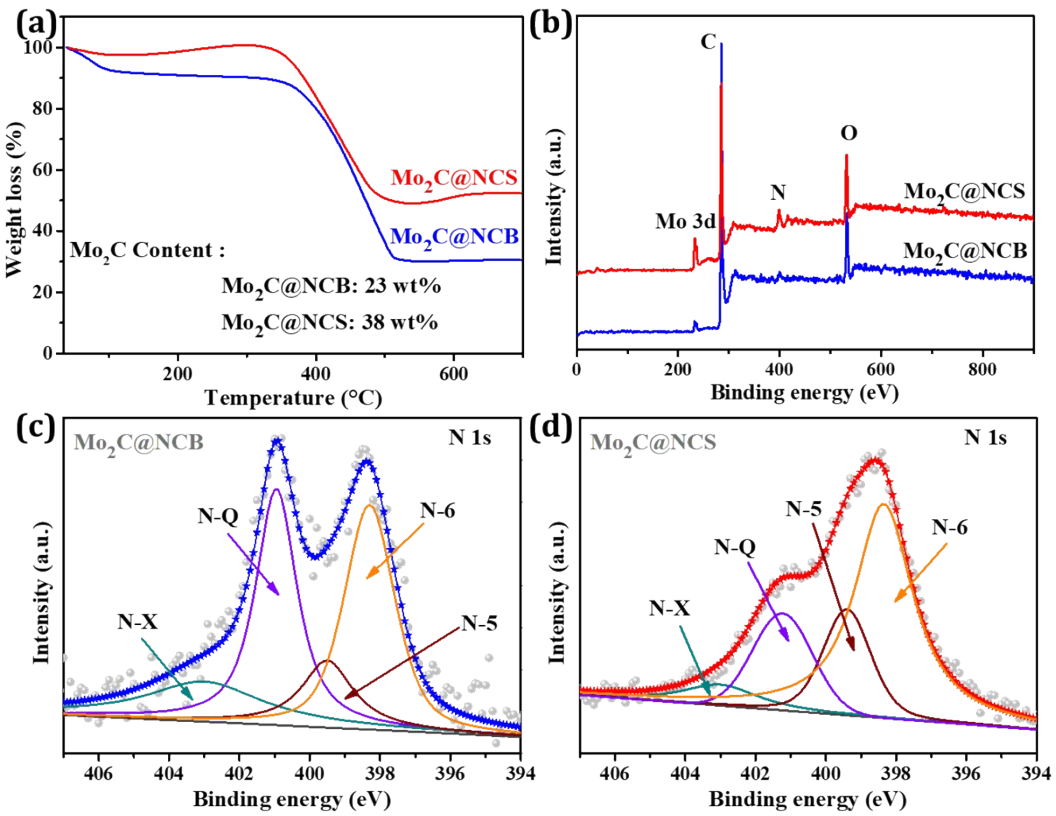

Fig. S4 (a) TGA curves, (b) XPS spectra, and core-level high-resolution N 1s spectra for (c) Mo_2C@NCB and (d) Mo_2C@NCS.

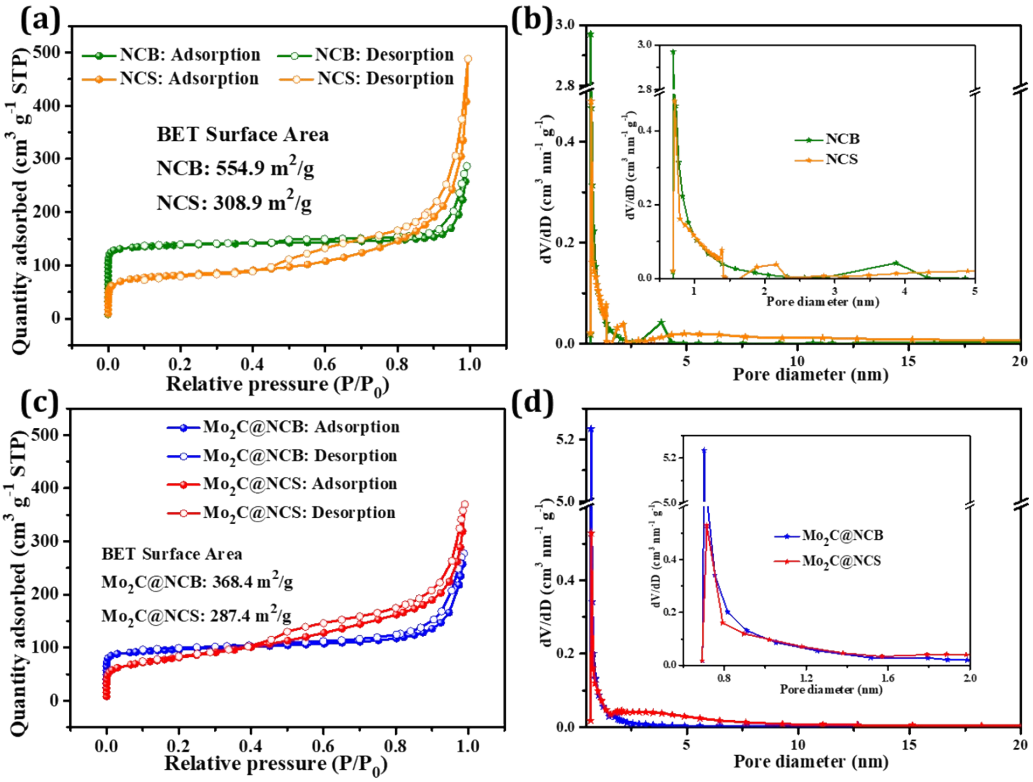

Fig. S5 (a, c) N_2 adsorption/desorption isotherms and (b, d) pore diameter distributions for (a, b) NCB and NCS, and (c, d) Mo_2C@NCB and Mo_2C@NCS.

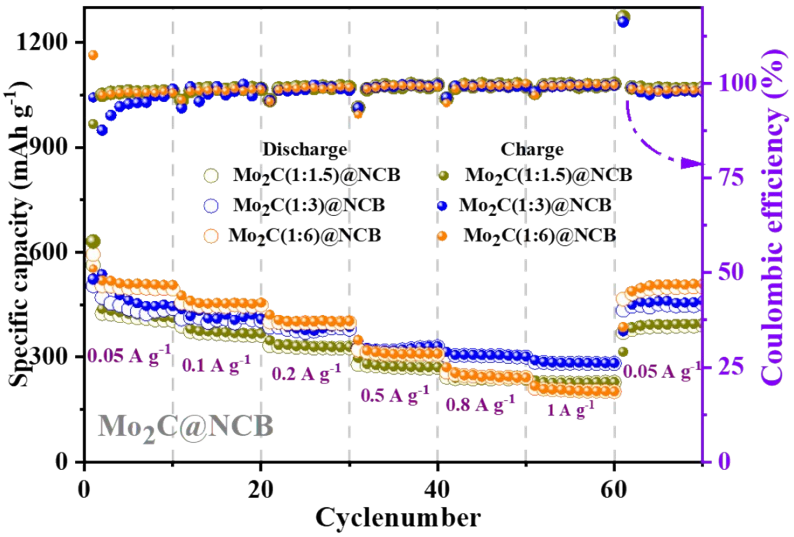

Fig. S6 Rate performance of Mo_2C@NCB-based anodes fabricated by the mass feed ratio of 1:1.5, 1:3, and 1:6 for PMo_{12} to PMDA-MDA comonomer salts. The lower amount of Mo_2C in Mo_2C@NCB leads a lower specific capacity, and the higher amount of Mo_2C in Mo_2C@NCB results in a higher initial capacity but an inferior rate performance. In contrast, the Mo_2C@NCB anode with a moderate loading (38%) of Mo_2C shows an optimal combination of specific capacity and rate capability, and was thus used as the anode of LICs in our work.

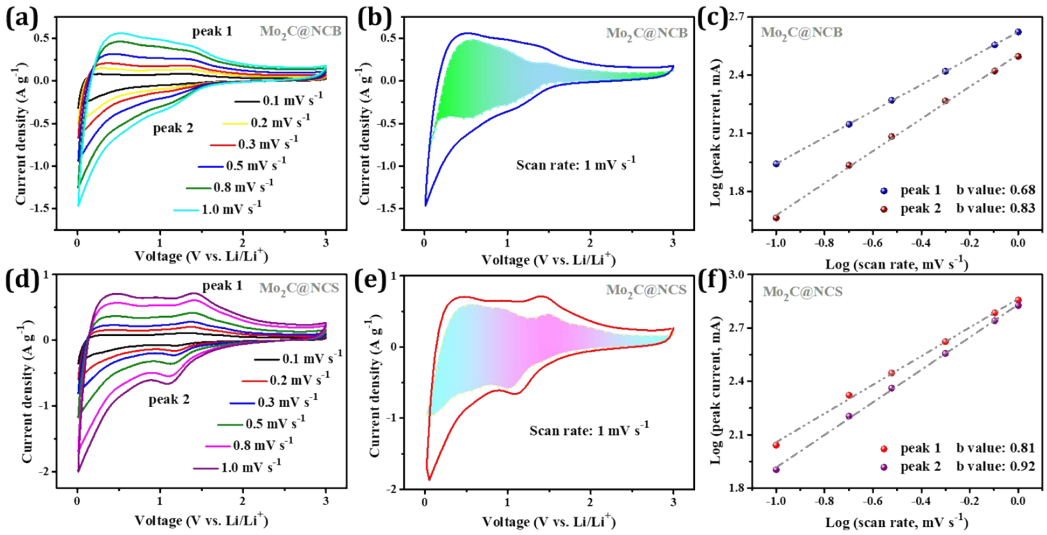

Fig. S7 (a, d) CV curves at scan rates of 0.1–1 mV s^{-1}, (b, e) the separation of capacitive and diffusion current at 1 mV s^{-1}, and (c, f) the log(*i*) *versus* log(*v*) plots and their fitting *b*-values for Mo_2C@NCB and Mo_2C@NCS anodes.

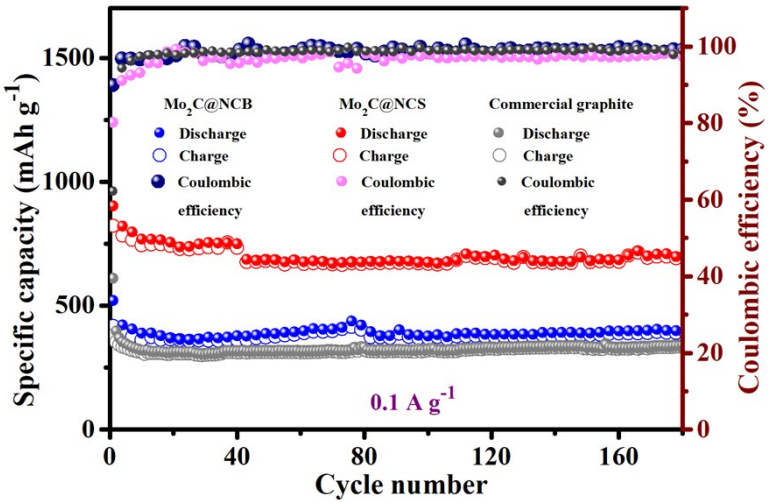

Fig. S8 Cycling performance of commercial graphite, and Mo_2C@NCB and Mo_2C@NCS anodes.

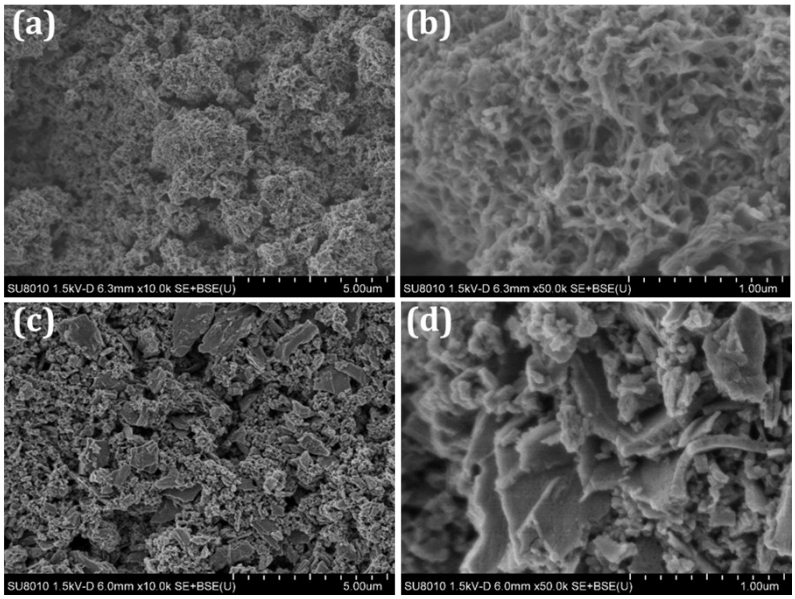

Fig. S9 SEM images of (a, b) Mo_2C@NCB and (c, d) Mo_2C@NCS anodes after running 180 cycles.

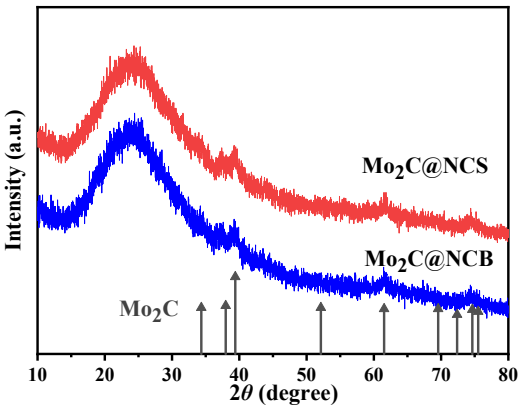

Fig. S10 XRD patterns of Mo_2C@NCB and (c, d) Mo_2C@NCS anodes after running 180 cycles.

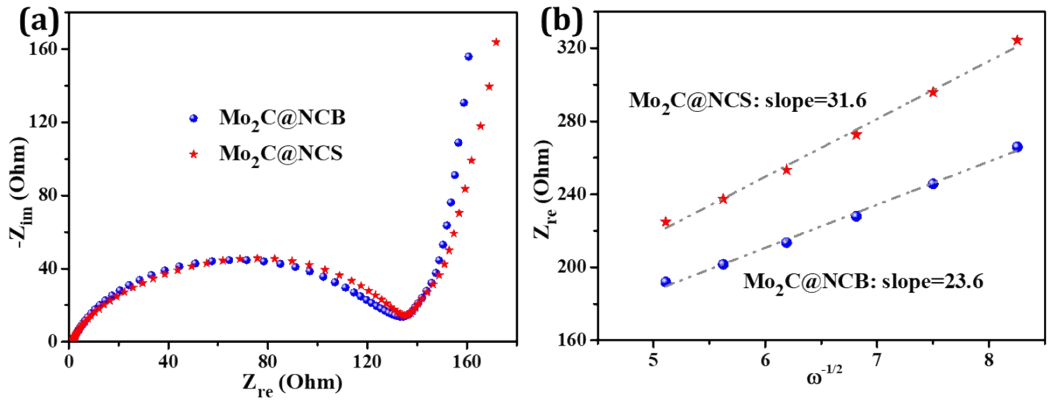

Fig. S11 (a) Nyquist plots, and (b) the relationship between the real part of the impedance (Z_{re}) and the reciprocal of the square root of frequency ($\omega^{-1/2}$) for Mo_2C@NCB and Mo_2C@NCS anodes.

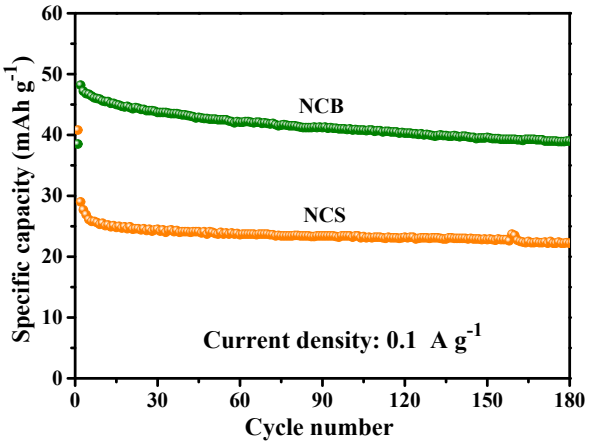

Fig. S12 Cycling stability of half-cell based on NCB and NCS electrodes at 0.1 A g^{-1}.

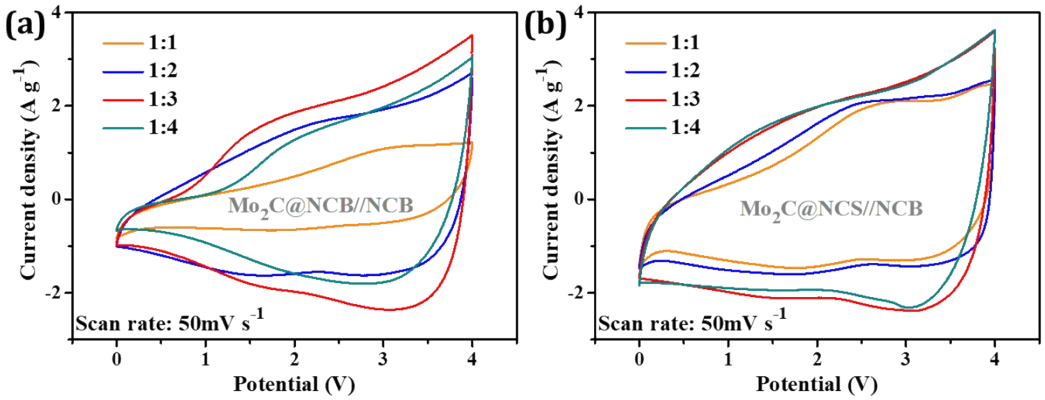

Fig. S13 CV curves of (a) Mo_2C@NCB//NCB and (b) Mo_2C@NCS//NCB devices fabricated with different mass ratio of active materials in two asymmetric electrodes system at 50 mV s^{-1}.

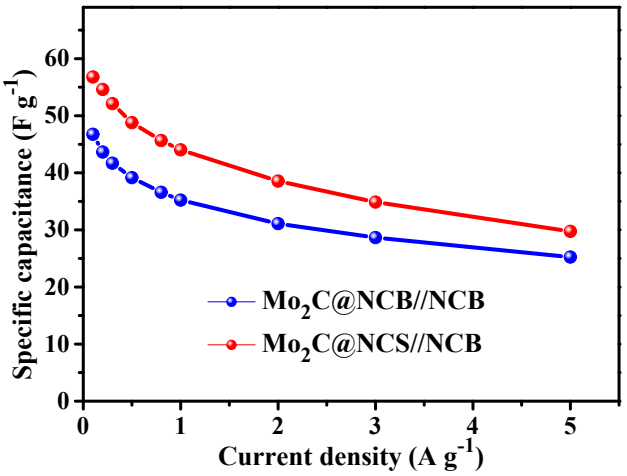

Fig. S14 Specific capacitances of both Mo_2C@NCB//NCB and Mo_2C@NCS//NCB LICs at different current densities.

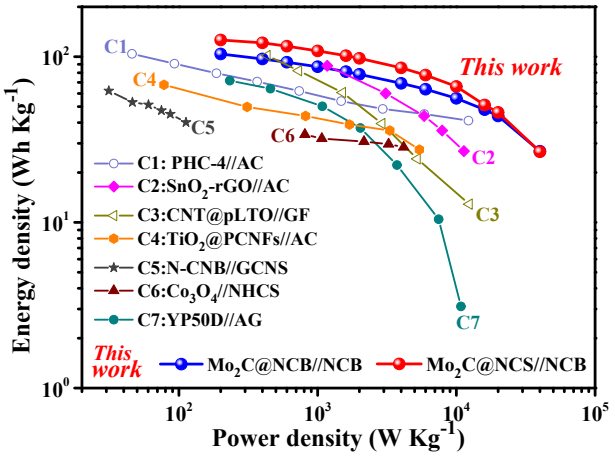

Fig. S15 Ragone plots of Mo_2C@NCB//NCB and Mo_2C@NCS//NCB devices and reported previously (**C1**,[2] **C2**,[3] **C3**,[4] **C4**,[5] **C5**,[6] **C6**,[7] and **C7**[8]).

Table S1 Initial capacity and cycling stability of Mo_2C@NCB and Mo_2C@NCS anodes and the previously-reported Mo_2C-contained anodes for LIBs

Anode	Mo_2C (wt.%)	Initial discharge capacity	Cycling stability	Ref.
MoO_2/Mo_2C	30	480 mAh g^{-1} at 200 mA g^{-1}	164.6% after 50 cycles at 200 mA g^{-1}	9
$MoO_2/Mo_2C/C$	54.9	1172 mAh g^{-1} at 100 mA g^{-1}	68.3 % after 100 cycles at 100 mA g^{-1}	10
Mo_2C-C	66.44	951.2 mAh g^{-1} at 100 mA g^{-1}	70.7% after 50 cycles at 100 mA g^{-1}	11
H-Mo_2C@C /NFs	26.5	1176.3 mAh g^{-1} at 100 mA g^{-1}	73.5% after 70 cycles at 100 mA g^{-1}	12
Mo_2C@OLC/a-C NCs	—	1065 mAh g^{-1} at 100 mA g^{-1}	66.5% after 100 cycles at 100 mA g^{-1}	13
MoO_2/Mo_2C/RG O	9.3	722 mAh g^{-1} at 50 mA g^{-1}	69.2% after 150 cycles at 50 mA g^{-1}	14
Mo_2C–NCNFs	57.86	1070.9 mAh g^{-1} at 100 mA g^{-1}	61.4% after 50 cycles at 100 mA g^{-1}	15
Mo_2C@NCB	**23**	**1043 mAh g^{-1} at 50 mA g^{-1}**	**86.3% after 180 cycles at 100 mA g^{-1}**	**This work**
Mo_2C@NCS	**38**	**1537 mAh g^{-1} at 50 mA g^{-1}**	**85.6% after 180 cycles at 100 mA g^{-1}**	

Table S2 Electrochemical performance of both Mo_2C@NCB//NCB and Mo_2C@NCS//NCS LICs and the previously-reported LICs

LICs	Potential (V)	Capacitance (C_{cell})	Rate capability	Cycling stability	Ref.
TiC//PHPNC	0~4.5	36 F g^{-1} at 0.2 A g^{-1}	8.3 F g^{-1} at 30 A g^{-1}	82% after 5000 cycles at 2 A g^{-1}	16
SC//AC/Li_3N	2~4	43.7 F g^{-1} at 0.05 A g^{-1}	14.9 F g^{-1} at 5 A g^{-1}	91% after 10,000 cycles at 0.5 A g^{-1}	17
$LiTi_2(PO_4)_3$//AC	0~3	16 F g^{-1} at 0.03 A g^{-1}	3 F g^{-1} at 0.09 A g^{-1}	60% after 250 cycles at 0.06 A g^{-1}	18
T-Nb_2O_5 MNSs/rGo //MC/rGo	0.5~3	45.9 F g^{-1} at 0.05 A g^{-1}	16.9 F g^{-1} at 10 A g^{-1}	82% after 4000 cycles at 1 A g^{-1}	19
$LiCrTiO_4$//AC	1~3	21 F g^{-1} at 0.4 A g^{-1}	4 F g^{-1} at 2 A g^{-1}	85.5% after 1000 cycles at 0.4 A g^{-1}	20
TiO_2 NBA //Graphene	0~3.8	41 F g^{-1} at 0.3 A g^{-1}	10.5 F g^{-1} at 10 A g^{-1}	73% after 600 cycles at 1 A g^{-1}	21
Graphene-wrapped LTO//AC	1~2.5	20.9 F g^{-1} at 0.1 mA cm^{-2}	6.4 F g^{-1} at 15 mA cm^{-2}	75% after 1000 cycles at 1 mA cm^{-2}	22
Mo_2C@NCB//NCB	**0~4**	**47 F g^{-1} at 0.1 A g^{-1}**	**25 F g^{-1} at 5 A g^{-1}**	**86% after 10,000 cycles at 5 A g^{-1}**	**This work**
Mo_2C@NCS//NCB	**0~4**	**57 F g^{-1} at 0.1 A g^{-1}**	**30 F g^{-1} at 5 A g^{-1}**	**80% after 10,000 cycles at 5 A g^{-1}**	

References

1. Y. Y. Chen, Y. Zhang, W. J. Jiang, X. Zhang, Z. Dai, L. J. Wan and J. S. Hu, *ACS Nano*, 2016, **10**, 8851.
2. Z. Yang, Y. Gao, Z. Zhao, Y. Wang, Y. Wu and X. Wang, *J. Power Sources*, 2020, **474**, 228500.
3. M. Arnaiz, C. Botas, D. Carriazo, R. Mysyk, F. Mijangos, T. Rojo, J. Ajuria and E. Goikolea, *Electrochim. Acta*, 2018, **284**, 542.
4. Y. Liu, W. Wang, J. Chen, X. Li, Q. Cheng and G. Wang, *J. Energy Chem.*, 2020, **50**, 344.
5. J. Zhang, H. Chen, X. Sun, X. Kang, Y. Zhang, C. Xu and Y. Zhang, *J. Electrochem. Soc.*, 2017, **164**, A820.
6. J.-T. Su, Y.-J. Wu, C.-L. Huang, Y.-A. Chen, H.-Y. Cheng, P.-Y. Cheng, C.-T. Hsieh and S.-Y. Lu, *Chem. Eng. J.*, 2020, **396**, 125314.
7. X. Wang, H. Xia, X. Wang, J. Gao, B. Shi and Y. Fang, *J. Alloys Compd.*, 2016, **686**, 969.
8. R. Lu, X. Ren, C. Zhan, C. Wang, R. Lv, W. Shen, F. Kang and Z.-H. Huang, *J. Alloys Compd.*, 2020, **835**, 155398.
9. H.-J. Zhang, K.-X. Wang, X.-Y. Wu, Y.-M. Jiang, Y.-B. Zhai, C. Wang, X. Wei and J.-S. Chen, *Adv. Funct. Mater.,* 2014, **24**, 3399.
10. M. Ihsan, H. Wang, S. R. Majid, J. Yang, S. J. Kennedy, Z. Guo and H. K. Liu, *Carbon*, 2016, **96**, 1200.
11. Q. Gao, X. Zhao, Y. Xiao, D. Zhao and M. Cao, *Nanoscale*, 2014, **6**, 6151.
12. M. Zhang, X. Huang, H. Xin, D. Li, Y. Zhao, L. Shi, Y. Lin, J. Yu, Z. Yu, C. Zhu and J. Xu, *Appl. Surf. Sci.*, 2019, **473**, 352.
13. X. Liu, Z. Li, S. Zhang, H. Long, H. Wei, H. Zhang, H. Li and C. Zhao, *Ceram. Int.*, 2017, **43**, 14446.
14. W. Devina, J. Hwang and J. Kim, *Chem. Eng. J.*, 2018, **345**, 1.
15. R. Li, S. Wang, W. Wang and M. Cao, *Phys. Chem. Chem. Phys.*, 2015, **17**, 24803.
16. H. Wang, Y. Zhang, H. Ang, Y. Zhang, H. T. Tan, Y. Zhang, Y. Guo, J. B. Franklin, X. L. Wu, M. Srinivasan, H. J. Fan and Q. Yan, *Adv. Funct. Mater.*, 2016, **26**, 3082.
17. C. Sun, X. Zhang, C. Li, K. Wang, X. Sun and Y. Ma, *Energy Storage Mater.*, 2020, **24**, 160.
18. V. Aravindan, W. Chuiling, M. V. Reddy, G. V. Rao, B. V. Chowdari and S. Madhavi, *Phys. Chem. Chem. Phys.*, 2012, **14**, 5808.
19. G. Ma, K. Li, Y. Li, B. Gao, T. Ding, Q. Zhong, J. Su, L. Gong, J. Chen, L. Yuan, B. Hu, J. Zhou and K. Huo, *Chem. Electro. Chem.*, 2016, **3**, 1360.
20. V. Aravindan, W. Chuiling and S. Madhavi, *J. Mater. Chem.*, 2012, **22**, 16026.
21. H. Wang, C. Guan, X. Wang and H. J. Fan, *Small*, 2015, **11**, 1470.
22. H. Kim, K.-Y. Park, M.-Y. Cho, M.-H. Kim, J. Hong, S.-K. Jung, K. C. Roh and K. Kang, *Chem. Electro. Chem.*, 2014, **1**, 125.